JOURNAL OF MECHANICAL ENGINEERING AND SCIENCES
ISSN: 2289-4659 e-ISSN: 2231-8380
VOLUME 20, ISSUE 3, 2026, 12354 - 12370
DOI: https://doi.org/10.15282/jmes.20.3.2026.7.0884

RESEARCH ARTICLE

# Optimization and prediction of wear in LM25–$B_4C$/EN31 tribopair using Taguchi method and machine learning model

**Zeeshan Ahmad[1]*, Sabah Khan[2]**

[1]Department of Mechanical Engineering, R V Institute of Technology Bijnor, Uttar Pradesh, India
[2]Department of Mechanical Engineering, Faculty of Engineering & Technology, Jamia Millia Islamia, New Delhi, India
Phone: +919650786020

**Abstract -** This study aimed to analyse the interfacial contact between LM25-B4C composite and steel EN 31 tribopairs via pin-on-disc wear tests. The Taguchi approach was employed to design the pin-on-disc experiments to evaluate the tribological properties of the material system. The optimal conditions for the lowest wear rate were identified at 12 wt.% reinforcement, a low load of 19.62 N, and a sliding distance of 1200 m. SEM micrographs show formation of a homogeneous α-aluminium dendrites network structure developed due to super-cooling of casting during solidification. energy dispersive spectroscopy spectrum of 12 wt.% B4C composite confirmed high content of ceramic elements which improved mechanical and wear properties. Coefficient of friction (COF) analysis showed a higher value reduction with 12 wt. %B4C additC addition, and its percentage reduction increased at higher load and with increase in sliding distance in all composites. Wear mechanisms transition from two-body abrasion and ploughing in the base alloy and lower-reinforced composites to three-body abrasion and plastic deformation in the 12 wt.% $B_4C$ composite. This transition is attributed to the high compressive strength of ceramic particles, which restrains severe delamination wear. Furthermore, four machine learning models predicted wear and COF, with polynomial regression performing best for wear rate and linear regression for COF.

**Article History**
Received : 27 March 2026
Revised : 20 July 2026
Accepted : 2 September 2026
Published : 30 September 2026

**Keywords**
*Tribo pair*
*Taguchi technique*
*Wear mechanics*
*Machine learning models*

## 1. Introduction

Aluminum alloys are preferred engineering materials for machine components in industrial and automotive industries. Particulate-reinforced aluminium matrix composites (AMCs) are attractive metal materials owing to their high strength, ductility, and toughness [1]–[3]. Depending on the nature of the contact between machine elements during motion transmission, tribological aspects are the main cause of failure in such components. These components are mostly designed to work in severe working environments, but aluminium alloys are susceptible to scratches and indentations, which become stress concentration points and lead to failure. Thus, to avoid untimely failures, aluminium matrix composites can be developed with tailor-made tribological properties by reinforcing them with ceramics. Ramarao and Padmanabhan [4] fabricated a boron carbide-reinforced aluminium alloy LM6 composite through a stir casting technique with 2.5–7.5% concentration of 30 µm boron carbide particles. The results showed increased hardness and ultimate compressive strength, whereas the density decreased with increasing wt.% of boron carbide. Similar results were obtained in studies on the mechanical properties of aluminium alloy Al 6061, Al 7075, and Al 2024 matrix composites reinforced with varying wt.% and vol.% of boron carbide [5]–[7]. Ahmad et al. [8] characterised and evaluated the microstructural and mechanical properties of LM 25 composites reinforced with silicon nitride and found improved mechanical properties owing to the homogeneous distribution of reinforcement particles and enrichment of silicon nitride particles. Rebba and Ramanaiah [9] developed Al 2024 aluminium alloy composites reinforced with 0–5 wt.% B4C, with increased hardness in the reinforced composite.% B4C, with an increase in hardness in the reinforced composite. Raviteja et al. [10] developed a 0–10 wt.% boron carbide-reinforced composites in an Al-Si12Cu matrix through the stir-casting route and showed improved hardness and tensile strength with increasing reinforcement. Yuvaraj et al. [11] produced aluminium alloy Al 5083 composites reinforced with B4Cwith particle sizes of micro 20 µm and nano 30–60 nm, using both one- and three-pass friction stir methods. The tribological results showed better wear resistance in composites with nanoparticles of 30–60 nm. Harichandran and Selvakumar [12] investigated the tribological and mechanical properties of 70 µm and 100 nm boron carbide (2–10 wt. %) reinforced aluminium composites prepared via stir casting with ultrasonic cavitation. The wear rate and coefficient of friction directly increased with an increase in load and were inversely proportional to the weight fraction of Bc. Qayyum et al. [13] applied the sloping plate method to improve the material properties of aluminium alloy LM25 in gravity die casting through grain modification. The influence of various speeds and pressures on the coefficient of friction of LM 25 and LM 25-granite composites was investigated; results showed that the coefficient of friction decreased with increasing sliding speed and applied pressure, as well as with granite reinforcement [14]. Researchers have studied the wear performance of tribopairs processed using different techniques to improve efficiency and prevent energy loss owing to tribological effects [15]–[22]. Vilaseca et al. [15] investigated the tribological properties of an aluminium-tool steel tribopair against different tool steel grades DIN 1.2344 (41 and 52 HRC), HTCS-150 (52 HRC), and HTCS-170 (52 HRC) and found that aluminium soldering was less trapped in HTCS steel compared to DIN 1.2344 and the wear and galling behaviour of tribopair at various temperatures were found dependent on system temperatures and wear occurred in form of pure abrasive to layer formation of aluminium debris [15]- [16]. Pujante et al. [16] investigated the aluminium alloy wear mechanism against tool steel with the effect of

***CORRESPONDING AUTHOR | Zeeshan Ahmad** | ✉ response.zeeshan@gmail.com
© 2026 The Authors. Published by Universiti Malaysia Pahang Al-Sultan Abdullah Press. This is an open access article under the CC BY-NC 4.0 license

surface finish on ball-on-disc at varying temperatures and observed that surface finish had a negligible effect on gross material transfer with no effect on the micro mechanism of material transfer. Zavos and Nikolakopoulos [17] studied the effect of surface irregularities on the piston ring-cylinder tribopair of a 2-stroke motor engine under hydrodynamic lubrication conditions and found that friction decreased with a worn ring profile, with mechanical stresses generated due to increased deformation. Chen et al. [18] investigated the dry sliding wear of a titanium alloy-AISI 52100 steel tribopair at loads of 50–250 N and temperatures of 25–600 °C. Severe to mild wear of titanium alloy pins resulted from the formation of tribo-layers containing tribo-oxides, especially Fe2O3. Li et al. [19] investigated the wear behaviour of the MoSi2 / Ti composite coating with brass, $ZrO_2$, GCr15, and WC tribo-pairs, and the results showed that the shear strength at the interface influenced the frictional behaviour, with a high coefficient of friction (COF) and high interfacial shear strength. Reddy et al. [20] investigated the tribological behaviour of a liner-ring tribopair using newly prepared biodegradable compressor oil prepared by an ultrasonication-based transesterification technique. Results showed improved tribological performance in terms of coefficient of friction, wear, and specific wear rate compared with SAE 30 grade compressor oil. Huttunen-Saarivirta et al. [21] studied the wear behaviour of aluminium alloy 6082 and tool steel H13 tribopair and found abrasion wear at a contact pressure of 510 MPa and severe adhesive wear at the high contact pressure. Stojanović et al. [22] analysed the effect of graphite on SiC-reinforced aluminium composites and found that low wt.% graphite addition exhibited improved wear performance. Wang et al. [23] reported the interfacial contact of aluminium alloy AA7475 and hardened steel H11 tribopair at elevated temperatures and found that COF increased with increasing sliding distance. Along with aluminium base metal matrix composites, researchers studied the wear behavior of cermets and ceramic composites and found that the presence of hard ceramic materials in the composition resulted in higher hardness and improved wear resistance [24].

Sahin [25] conducted a statistical analysis using Taguchi techniques and determined the significance of various factors through analysis of variance (ANOVA). Their study highlighted the substantial impact of these factors on the wear behaviour observed in the pin-on-disc wear test. Among the variables, the weight percentage of reinforcement was identified as the most influential factor on wear. Adding an optimum amount of reinforcement led to a uniform distribution within the fabricated composite. Optimising process parameters and identifying the most significant influencing factors are essential steps in experimental research, as they enhance the understanding of each variable's contribution to the overall performance of the process [26]–[28]. In this context, numerous researchers have applied various optimisation techniques and statistical methods to improve the material behaviour and system performance [29]–[31]. However, the application of machine learning (ML) models in tribological experiments remains limited, motivating further research aimed at process parameter optimisation using advanced data-driven approaches. This study investigates the wear behaviour of aluminium alloys and their composites against an EN 31 steel tribopair under varying loads and sliding distances, with commercial applications. Understanding the wear characteristics between mating components is crucial for machine operations, as relative motion under load leads to material loss, reduced power transmission efficiency, and decreased tribopair operational life. This study also incorporates machine learning models, including linear regression, polynomial regression, random forest, and Gaussian process regression, to predict wear behaviour based on experimental data.

## 2. Materials and Methods

This section outlines the methodology adopted for the fabrication of LM25 aluminium alloy reinforced with $B_4C$ (boron carbide) composites using the stir-casting technique, along with the procedures for the characterisation and evaluation of the tribological properties. The methodology encompasses material selection, composite fabrication via stir casting, specimen preparation, and assessment of tribological behaviour. Additionally, statistical validation of the experimental data, evaluation of the worn surface morphology, and analysis of the dissipated energy during wear testing were included to ensure a comprehensive understanding of the performance of the material under tribological conditions.

### 2.1 Material Preparation

In this study, commercially available LM 25 alloy was employed as the matrix and boron carbide as reinforcement, as it is one of the hardest known ceramics [32]. Optical emission spectroscopy was performed on LM 25 aluminium alloy to determine the chemical composition, as listed in Table 1. We fabricated an aluminium matrix composite using the stir casting technique, as shown in Figure 1. The method involves the melting of LM 25 matrix with continuous stirring followed by the addition of preheated boron carbide particles (400 °C for 30 minutes) [33]. The initial temperature was 500 °C, gradually increased to 850 °C, then poured into a preformed cavity, cooled, and allowed to solidify. This is an easy and economical technique for fabricating composites; however, agglomeration of reinforcement particles is a problem that can be minimised by vigorous stirring at high temperatures. For this study, the molten mixture was poured into a cylindrical steel mould (20 mm in diameter and 60 mm in length) and allowed to cool. Three sets of LM 25 composites with weight fractions of 4 wt.%, 8 wt.% and 12 wt.% of boron carbide were fabricated. The mechanical properties of the fabricated composites were also analysed [34]. The hardness of the composites enhanced with the addition of reinforcement; the presence of hard particles enhances the wear resistance by reducing the mean free path of soft particles or crack propagation. These reinforced hard particles act as load-supporting members in composites, can carry the normal loads, and prevent the softer matrix from becoming directly involved in the wear process. Brittle fracture morphology was observed in the composites with higher wt.%B4C added composite.

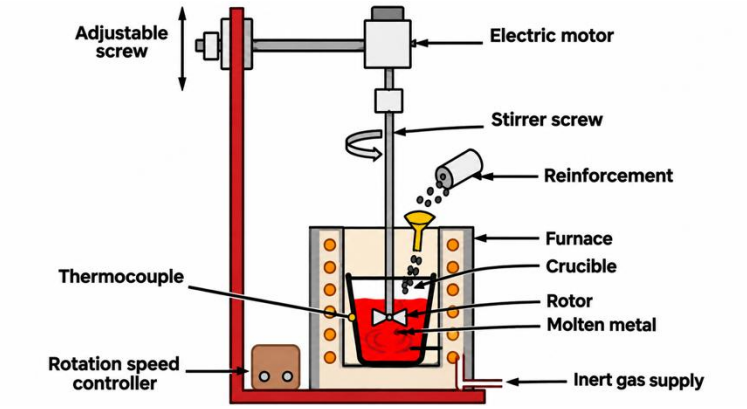


Figure1. Schematic view of stir casting set-up

Table 1. Chemical composition of aluminium alloy LM 25

| Chemical composition (%) | Value | Chemical composition (%) | Value |
|---|---|---|---|
| Si | 6.49 | Mn | 0.32 |
| Cu | 0.18 | V | 13 |
| Mg | 0.072 | Ti | 0.143 |
| Fe | 0.432 | Sn | 0.046 |
| Zn | 0.056 | Bi | 0.005 |
| Ni | 0.073 | Pb | 0.103 |
| Al | 92.09 | | |

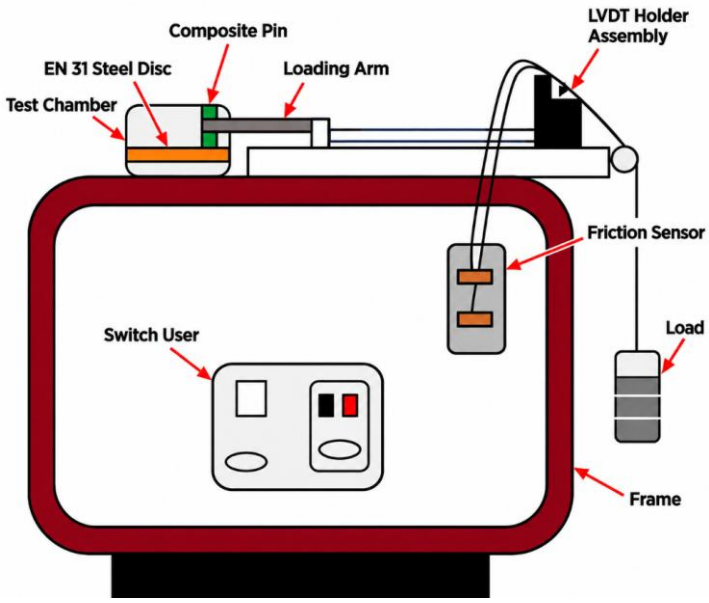


Figure 2. Schematic view of pin-on-disc apparatus

Wear tests were performed under ambient conditions using a pin-on-disc tribometre for aluminium alloy composites–steel tribopairs (Figure 2) at a constant sliding velocity and at various sliding distances with varying normal loads. The pin was made of LM 25 composites, cylindrical (12 mm in diameter and 30 mm in length), and pressed against a rotating counter flat EN 31 steel disc (165 mm in diameter and 8 mm thick). Surface preparation, such as grinding and lapping, was performed on the disc to make the surface hard and smooth. The contact surface of the pin was also smoothed. Pin wear was measured as weight loss; the pin specimens were weighed before and after the test on a weighing machine with a least count of 0.00001 g. The pin-on-disc tribometre was equipped with a high-quality frictional sensor to measure the frictional force at the contact surface. We used the frictional force to calculate the coefficient of friction (Table 2). We repeated the wear tests three times for each composite sample to maintain accuracy. At the start of the experiment, the disc and composite pin surfaces were cleaned with acetone. To maintain consistent input parameters, the normal applied load and relative speed of the disc were kept constant during the running period. The experiment was started by holding the composite pin in a well-designed holder on the machine. The disc was maintained at a fixed rotational speed, and the track diameter was set according to the requirements of each experiment. A pulley-and-wire system applied the normal

load using a dead weight. Table 3 lists the test parameters. Scanning electron microscopy (SEM) with energy dispersive spectroscopy (EDS) was used to analyse the microstructure of the fabricated composites [35].

Table 2. Parameter of pin-on-disc tribometer

| Parameters | Value | |
|---|---|---|
| Wear track diameter (mm) | 50-150 mm | |
| | Range (rpm) | 200-2000 |
| Disc rotation speed | Sensor | Drive Output |
| | The least count (rpm) | 1 |
| | Range (Kg) | 0-20 |
| Load Parameters | Specification | 20 Kg beam type load cell |
| | Least count (Kg) | 0.01 |
| | Range (mm) | 2 |
| Machine Parameters | Sensor | LVDT, Syscon |
| | Least count (µm) | 0.1 |

Table 3. Parameters for the wear test

| S. No. | Test condition | Value |
|---|---|---|
| 1 | Pin diameter, height | 32, 12 |
| 2 | Disc diameter, height | 165, 8 |
| 3 | Sliding velocity (m/s) | 2 |
| 4 | Track diameter (mm) | 70, 90, 110, 130, 150 |
| 5 | Rotation speed of disc (rpm) | 255, 295, 348, 425, 550 |
| 6 | Sliding distance (m) | 1200, 1800, 2400 |
| 7 | Normal load (N) | 19.6, 39.24, 58.86 |
| 8 | Temperature (°C) | 25 |

**2.2 Statistical Validation**

In this study, the Taguchi technique was used to statistically validate the specimens using Minitab design software. In this approach, the signal-to-noise (S/N) ratio is the primary metric for determining the optimal combination of variables. Correlation studies were also conducted to develop a regression equation and evaluate the model's fit. The experimental data were validated, and an analysis of variance was performed to identify the significance of the variations observed during the experimental trials. Table 4 lists the experimental parameters, and Table 5 presents the design of the experiments based on the Taguchi method.

Table 4. Parameters for the wear test

| S. No. | Factors | Level 1 | Level 2 | Level 3 | Level 4 |
|---|---|---|---|---|---|
| 1 | Reinforcement (wt.)% | 0 | 4 | 8 | 12 |
| 2 | Load (N) | 19.62 | 39.24 | 58.86 | -- |
| 3 | Sliding Distance (m) | 1200 | 1800 | 2400 | -- |

**2.3 Machine Learning Method**

Various machine learning techniques have been employed to analyse the wear behaviour and coefficient of friction of fabricated aluminum-based composites. To enhance the predictive performance of these techniques, the min-max scaling method was applied to normalise the experimental data. Based on a comprehensive literature survey, this study utilised linear, polynomial, random forest, and Gaussian process regressions to model and predict the tribological properties of the composites.

***2.3.1 Linear regression technique***

Linear regression is a statistical technique that measures the correlation between two or more independent variables and a dependent variable, with the goal of analysing the impact of the independent variables on the target outcome. The ordinary least squares (OLS) method is the most commonly used approach for estimating the parameters of linear regression models. In this study, linear regression was employed to predict the wear and coefficient of friction of the fabricated aluminium-based composites using key input parameters, such as the applied load, reinforcement percentage, and sliding distance. The general form of the linear regression model is

$$y = \delta_0 + \delta_1 x_1 + \delta_2 x_2 + \cdots \ldots \ldots \ldots \ldots \ldots \ldots \ldots \ldots \ldots \delta_n x_n + \epsilon \quad (1)$$

$$y = \delta_0 + \sum_{i=1}^{n} (\delta_i x_i) + \epsilon \quad (2)$$

where $y$ = predicted value (e.g. wear, COF), $\delta_0$ = intercept; $\delta_1, \delta_2, \delta_3$ = coefficient of each parameter and $\epsilon$ = error

Table 5. Input parameter and output responses

| S. No. | Reinforcement (wt.)% | Load (N) | Sliding Distance (m) | Wear (mg) | COF |
|---|---|---|---|---|---|
| 1 | 0 | 19.62 | 1200 | 0.0097 | 0.3102 |
| 2 | 0 | 19.62 | 1800 | 0.014 | 0.3186 |
| 3 | 0 | 19.62 | 2400 | 0.0186 | 0.3194 |
| 4 | 0 | 39.24 | 1200 | 0.012 | 0.318 |
| 5 | 0 | 39.24 | 1800 | 0.0185 | 0.323 |
| 6 | 0 | 39.24 | 2400 | 0.0253 | 0.329 |
| 7 | 0 | 58.86 | 1200 | 0.0135 | 0.322 |
| 8 | 0 | 58.86 | 1800 | 0.0221 | 0.327 |
| 9 | 0 | 58.86 | 2400 | 0.028 | 0.33 |
| 10 | 4 | 19.62 | 1200 | 0.0036 | 0.3056 |
| 11 | 4 | 19.62 | 1800 | 0.0062 | 0.3086 |
| 12 | 4 | 19.62 | 2400 | 0.0088 | 0.309 |
| 13 | 4 | 39.24 | 1200 | 0.0062 | 0.312 |
| 14 | 4 | 39.24 | 1800 | 0.0112 | 0.32 |
| 15 | 4 | 39.24 | 2400 | 0.015 | 0.319 |
| 16 | 4 | 58.86 | 1200 | 0.0086 | 0.316 |
| 17 | 4 | 58.86 | 1800 | 0.0162 | 0.323 |
| 18 | 4 | 58.86 | 2400 | 0.0202 | 0.324 |
| 19 | 8 | 19.62 | 1200 | 0.0028 | 0.3015 |
| 20 | 8 | 19.62 | 1800 | 0.0057 | 0.3045 |
| 21 | 8 | 19.62 | 2400 | 0.0084 | 0.305 |
| 22 | 8 | 39.24 | 1200 | 0.0048 | 0.307 |
| 23 | 8 | 39.24 | 1800 | 0.011 | 0.321 |
| 24 | 8 | 39.24 | 2400 | 0.0135 | 0.31 |
| 25 | 8 | 58.86 | 1200 | 0.0071 | 0.311 |
| 26 | 8 | 58.86 | 1800 | 0.0148 | 0.315 |
| 27 | 8 | 58.86 | 2400 | 0.0183 | 0.317 |
| 28 | 12 | 19.62 | 1200 | 0.0023 | 0.2987 |
| 29 | 12 | 19.62 | 1800 | 0.005 | 0.3014 |
| 30 | 12 | 19.62 | 2400 | 0.0076 | 0.3015 |
| 31 | 12 | 39.24 | 1200 | 0.0041 | 0.301 |
| 32 | 12 | 39.24 | 1800 | 0.009 | 0.3 |
| 33 | 12 | 39.24 | 2400 | 0.012 | 0.304 |
| 34 | 12 | 58.86 | 1200 | 0.0056 | 0.306 |
| 35 | 12 | 58.86 | 1800 | 0.0122 | 0.31 |
| 3 | 12 | 58.86 | 2400 | 0.0163 | |

### *2.3.2 Polynomial regression technique*

Polynomial regression is a form of regression analysis in which the relationship between the independent variable and the dependent variable is modelled as an nth-degree polynomial. Instead of fitting a straight line, polynomial regression fits a curve that can capture more complex nonlinear relationships. The model takes the form:

$$y = \delta_0 + \delta_1 x + \delta_2 x^2 + \delta_3 x^3 \ldots\ldots\ldots\ldots\ldots\ldots\ldots\ldots\ldots \delta_n x^n + \epsilon \quad (3)$$

$$y = \delta_0 + \sum_{i=1}^{n} (\delta_i x_i^n) + \epsilon \quad (4)$$

where $y$ is the dependent variable (e.g., wear or COF), $x$ is the independent variable, $\delta_0$ , $\delta_1, \delta_2, \delta_3$ are the coefficient of each parameter and $\epsilon$ = error

### *2.3.3 Random forest regression*

Random Forest Regression is a supervised machine learning technique that uses an ensemble of decision trees to predict continuous outputs. It is based on the approach of Bootstrap Aggregating (Bagging), where multiple decision trees are trained on different random subsets of the training data (with replacement), and their outputs are averaged to produce the final prediction.

$$Y_{RF} = \frac{1}{N}\sum_{i=1}^{N} h_n(x) \tag{5}$$

where, $y_{RF}$ = final predicted value; N = number of trees; and $h_n(x)$ = prediction from the n-th tree.

### *2.3.4 Linear Gaussian process regression*

Gaussian regression is a technique that is mostly used for nonlinear problems. In this approach, a Gaussian distribution is automatically identified for the random variable from all the input and output data. The trained data were used as input by the Gaussian process, which created variations for all attainable functions. The Gaussian process used in this approach is characterised by the kernel function $\ker(\dot{y}, \dot{y}')$ and the probability function of the mean function $n(\dot{y})$.

$$F(\dot{y}) = GP\big(n(\dot{y}), \ker(\dot{y}, \dot{y}')\big) \tag{6}$$

where $n(\dot{y})$ is an accurate measure of the central tendency in the Gaussian model. The Gaussian regression model that defines the input and output correlation is defined as

$$y_{GP} = G(y) + \epsilon \tag{7}$$

## 3. Results and Discussion

The SEM image of the LM 25 cast alloy indicated structural homogeneity (Figure 3). The microstructure of the cast LM 25 revealed the formation of a homogeneous α-aluminium dendrite network structure, which developed owing to the supercooling of the casting during solidification. The EDS spectrum showed peaks for various constituents of the LM 25 aluminium alloy, confirming the presence of Si, Mg, Cu, and Zn. The SEM image of the LM25-4 wt.% B4C composite reveals homogeneity in the composition of the fabricated composite (Figure 4(a)). The dark spots are B4C particles surrounded by a dark gray matrix. The dispersion of the BCPs was uniform, and no clusters were observed in the micrographs of the samples. SEM micrographs of LM 25-8,12 wt.%B4C composites showed that the dispersion of boron carbide particles was uniform, with no clustering of reinforcement particles (Figure 4(b-c)). The gray spots surrounded by dark gray indicate dendritic growth during solidification, and shrinkage was observed at some locations; however, the cause of this defect is not clear at this temperature. The direct contact between the molten LM 25 alloy and B4C particles may have resulted in the formation of Al4C3 at the interface between the two.

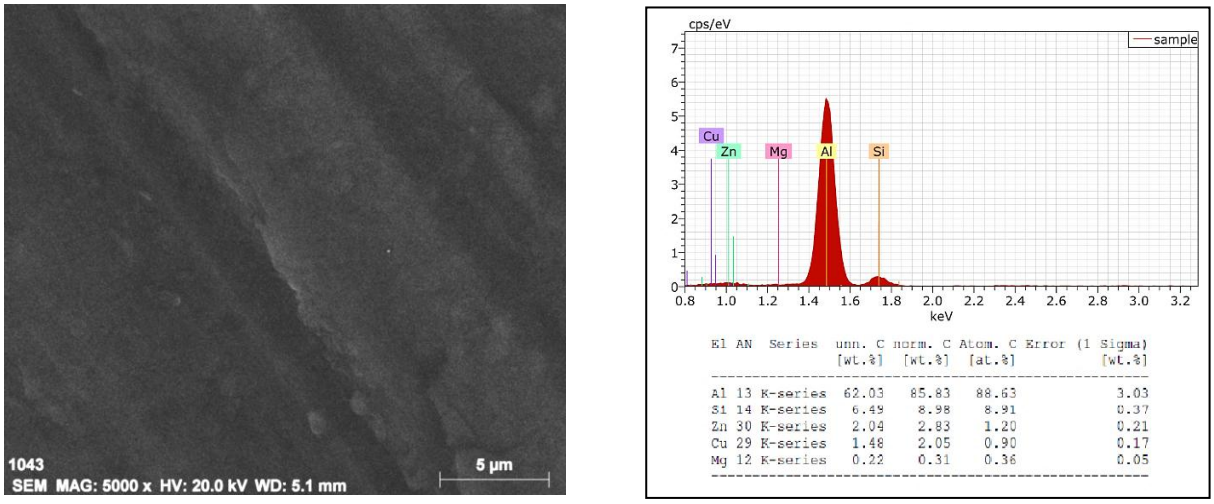


Figure 3. SEM micrograph and EDS spectrum of casted LM 25 alloy

EDS analysis was performed at different points on all composites to study the presence of various constituents and their effects on the mechanical and wear properties. The EDS spectrum showed distinct peaks for the constituent elements, confirming the presence of boron, carbon, and Mg in the Al alloy matrix. The EDS spectrum of the LM 25 composites reinforced with 4 wt.% B4C revealed 13.62 wt.% boron, 54.48 wt.% carbon, and 31.47 wt.% aluminium, which further increased for boron and decreased for aluminium in the 12 wt.% B4C-added composite, as shown in Figure 5(a). Energy-dispersive spectrometer analysis revealed that as the reinforcement percentage increased, the wt.% of hard boron particles increased, improving wear behaviour owing to their high hardness and compressive strength.

### 3.1 Taguchi Analysis

The primary objective of this study was to develop composite materials with enhanced wear resistance. To evaluate the effects of various parameters, the signal-to-noise (S/N) ratio was analysed using the "smaller-is-better" criterion, which is appropriate for minimising wear. The S/N ratio results (Table 6) indicate that the reinforcement percentage is the most

influential factor, as it shows the highest delta value, followed by the applied load and sliding distance. In addition, Analysis of Variance was conducted at a 95% confidence level (significance level of 0.05) to identify the parameters that significantly affect wear resistance. According to the ANOVA results (Table 7), sliding velocity was the most significant factor, contributing 36.14% to the variation in wear resistance, followed by reinforcement percentage (28.66%) and load (23.57%).

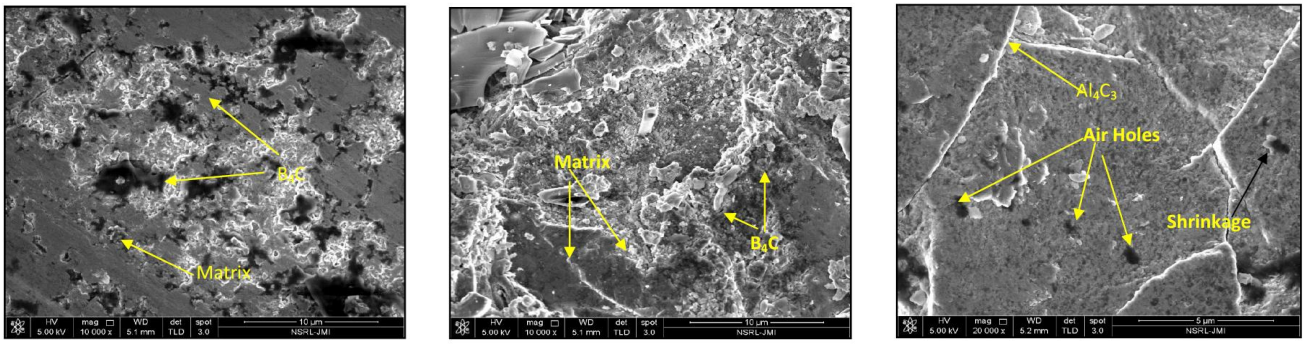


(a) (b) (c)

Figure 4. SEM micrograph (a) LM25–4 wt.% B4C composite; (b) LM25- 8 wt.% B4C composite; (a) LM25- 12 wt.% B4C composite

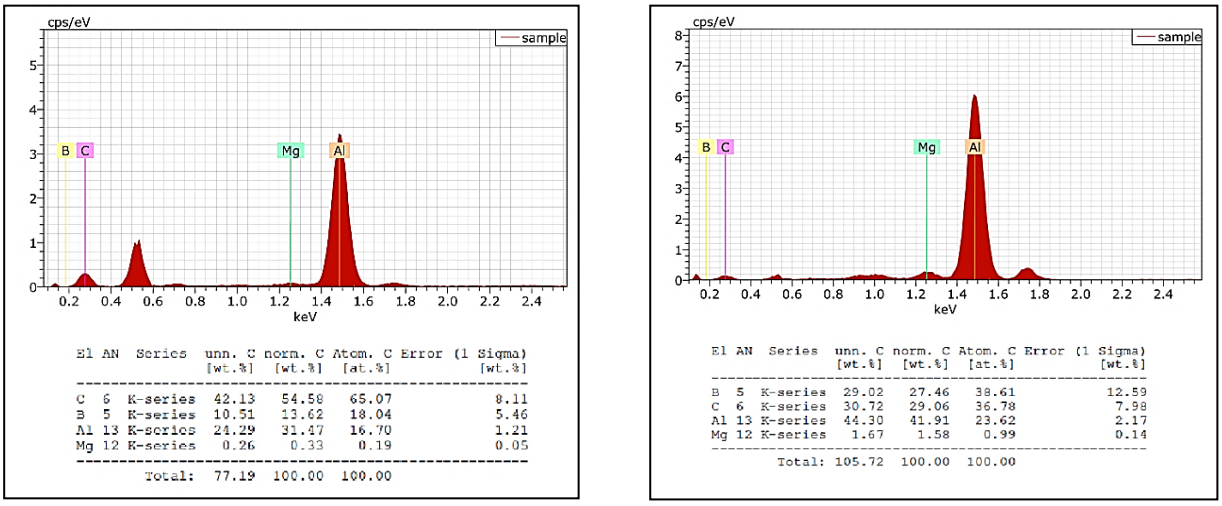


(a) (b)

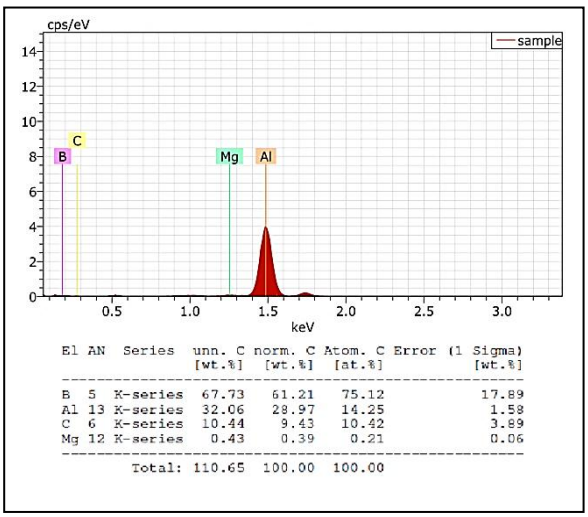


(c)

Figure 5. EDS spectra (a) LM25- 4 wt.% B4C composite; (b) LM25- 8 wt.% B4C composite; (c) LM25- 12 wt.% B4C composite

Table 6. Response of signal to noise ratio

| Level | Reinforcement (wt.%) | Load (N) | Sliding Distance (m) |
|---|---|---|---|
| 1 | 12.84 | 13.27 | 13.21 |
| 2 | 13.03 | 13.08 | 13.06 |
| 3 | 13.17 | 12.96 | 13.04 |
| 4 | 13.36 | --- | --- |
| Delta | 0.51 | 0.3 | 0.17 |
| Rank | 1 | 2 | 3 |

Table 7. Analysis of variance for means

| Source | DF | Seq SS | Adj SS | Adj MS | F-Value | P-Value | Contribution |
|---|---|---|---|---|---|---|---|
| Reinforcement | 1 | 0.000412 | 0.000039 | 0.000039 | 15.04 | 0.001 | 28.66% |
| Load | 1 | 0.000339 | 0.000137 | 0.000137 | 52.86 | 0.000 | 23.57% |
| Sliding Distance | 1 | 0.000520 | 0.000270 | 0.000270 | 104.57 | 0.000 | 36.14% |
| Reinforcement* Reinforcement | 1 | 0.000079 | 0.000079 | 0.000079 | 30.63 | 0.000 | 5.51% |
| Reinforcement* Load | 1 | 0.000001 | 0.000001 | 0.000001 | 0.28 | 0.598 | 0.05% |
| Reinforcement* Sliding Distance | 1 | 0.000012 | 0.000012 | 0.000012 | 4.78 | 0.037 | 0.86% |
| Error | 29 | 0.000075 | 0.000075 | 0.000003 | | | 5.21% |
| Total | 35 | 0.001438 | | | | | 100.00% |

The variations in wear for the different composites with increasing weight % of reinforcement, applied load, and sliding distance are shown in Figure 6. Majorly following three observations have been made. The mass loss was reduced for all three 4–12 wt.%% B4C-reinforced composites compared to the base alloy. Among the 4–12 wt.% B4C-reinforced composites, the 12 wt.% B4C-reinforced composite showed the greatest mass-loss reduction. The mass loss reduction percentage was higher for all composites at a low sliding distance of 1200 m. The mass loss for the composite reinforced with 4 wt.% B4C reduced to 62.89%, 55.71% and 52.69%, for composite sample reinforced with 8 wt.% as 71.13%, 59.29% and 54.84% and for composite sample reinforced with 12 wt.% as 76.29%, 64.29% and 59.14% compared to unreinforced aluminium alloy sample with increase in sliding distance from 1200m-2400m. Similarly, wear varied across composites as sliding distance increased at a constant load of 38.24N. The mass loss at each point for the composite sample reinforced with 4 wt.% decreases as 48.33%, 39.4% and 40.7%, for composite sample reinforced with 8 wt.% as 60%, 40.54% and 46.64%; and for the composite sample reinforced with 12 wt.% as 65.83%, 51.35% and 51.78% compared to the unreinforced aluminium alloy composite sample with increase in sliding distance. A similar trend in variation of mass loss for different composites with an increase in sliding distance at a constant load of 58.86N. With the three major observations mentioned above at particular loads, on comparison at three loads it has been found that wear loss reduction is higher at the lower load of 19.6 N. This wear rate in composites reduced due to a reduction in the actual contact area of the matrix reduced as the volume fraction of boron carbide particles increased; it may be attributed to the dispersion of coarser and larger size of boron carbide particles because longer dispersed particles do not easily breakdown and hard boron carbide particles resisted micro-cutting action by acting as load-bearing elements [36-42]. The results indicate that the optimal parameter settings for minimising wear are: reinforcement content at 12 wt.%, applied load of 19.62 N, and a sliding distance of 1200 m.

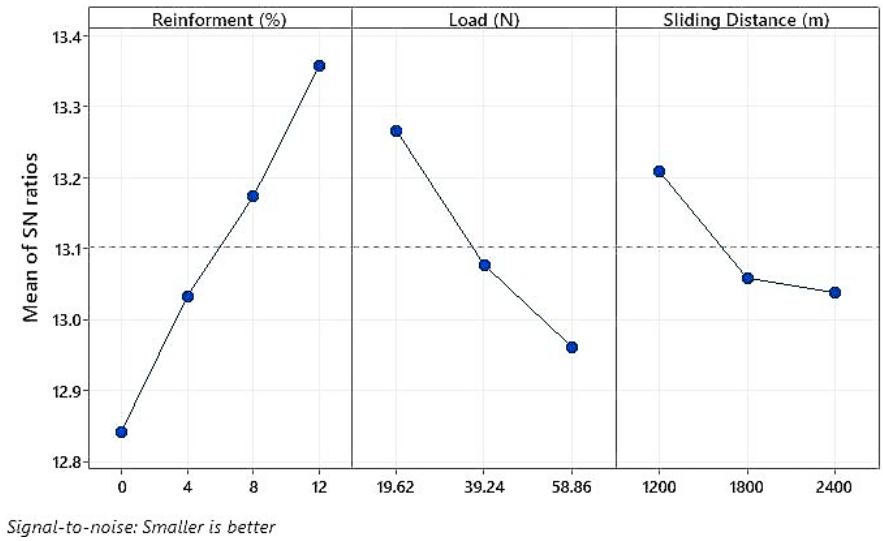


Figure 6. Effect of various factors on wear rate

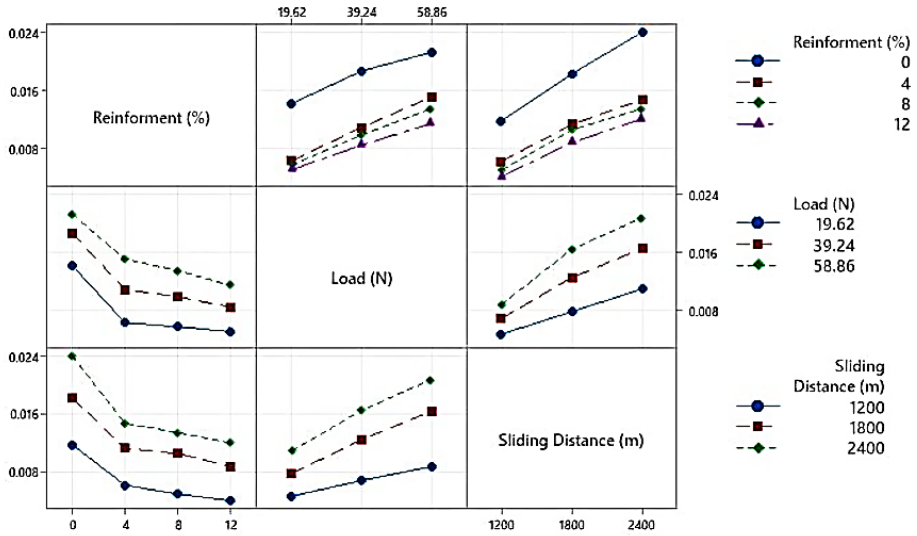


Figure 7. Interaction plots for means

The interaction plot for wear, as illustrated in Figure 6, demonstrates the combined effects of reinforcement percentage, applied load, and sliding distance on the wear behaviour of the developed materials. The results clearly indicate improved wear resistance with increasing reinforcement percentage across all composite samples. Although the wear rate increases with sliding distance for all materials, it is significantly higher in the unreinforced aluminium alloy compared to the composite samples. Among the composites, the sample reinforced with 12 wt.% boron carbide ($B_4C$) exhibits the most superior wear resistance, highlighting the beneficial effect of B4C reinforcement on the tribological properties of the aluminium matrix composites. The interaction between applied load and reinforcement percentage shows that the wear rate increases with applied load, rising from 19.62 N to 58.86 N. However, a linear reduction in wear rate is observed with increasing reinforcement content, and the composites consistently outperform the unreinforced aluminium alloy under all loading conditions. Furthermore, increasing sliding distance increases the wear rate for all samples, particularly under higher loads. The composite containing 12 wt.% $B_4C$ recorded the minimum wear at a load of 19.62 N and a sliding distance of 1200 m. As the sliding distance increased from 1200 m to 2400 m, the wear rate escalated for all samples; nonetheless, the 12 wt.% reinforced composite continues to exhibit the lowest wear under all tested conditions. These findings confirm that $B_4C$ reinforcement plays a significant role in enhancing the wear resistance of aluminium matrix composites, particularly under lower loads and shorter sliding distances.

Figure 7 presents four residual plots to evaluate the residuals of the statistical model associated with the mean values. A normal probability plot was used to assess whether the residuals followed normal distribution. Ideally, the residuals should lie along the diagonal. Although slight deviations appear at the extremes, the residuals are approximately normally distributed, as most of the points align closely with the line. The residuals vs. fitted values plot compares the residuals to the predicted (fitted) values. This plot helps detect potential issues such as heteroscedasticity (non-constant variance) or nonlinearity. In this case, the residuals appeared randomly scattered around zero with no apparent pattern, indicating that the model did not exhibit significant non-linearity or unequal variance. The histogram shows the frequency distribution of the residuals. The distribution is generally symmetric and centred around zero, although there is a slight skewness. The overall bell-shaped pattern suggests that the residuals approximately followed a normal distribution with minor deviations. The residuals vs. order plot shows residuals by order of data collection, helping to identify potential autocorrelation or time-related biases. The residuals fluctuated randomly around zero, indicating no significant correlation between successive observations and confirming the independence of the residuals. Collectively, these residual plots show that the model satisfies key assumptions, such as normality, linearity, constant variance, and independence, supporting the model's reliability and validity in explaining observed data.

Figure 8 (a)–(c) show the variation in the coefficient of friction of the composite with sliding distance under various loads and different percentages of reinforcement. Figure 8(a) shows the variation of the COF for different samples with increasing sliding distance at a constant load of 19.62 N. The coefficient of friction plots for the composite samples are linear with the sliding distance. The coefficient of friction at each point for the composite sample reinforced with 4 wt.% decreases as 1.48%, 3.14% and 3.25% with increase in load 1200-2400m, for composite sample reinforced with 8 wt.% as 2.80%, 4.42% and 4.5% and for composite sample reinforced with 12 wt.% as 3.71%, 5.40% and 5.60% as compared to unreinforced aluminium alloy LM 25 sample with increase in sliding distance from 1200-2400 m. Figure 8(b-c) shows a similar trend in the variation of the coefficient of friction for different composites with an increase in sliding distance at constant loads of 38.24 N and 58.84 N. In Figure 8(a-c), the variation of the coefficient of friction increases at the start and then becomes constant and remains constant with further increase in sliding distance. Kumar and Wani [43] studied the wear performance in dry and wet conditions for Al-Si composites and found that lubrication reduces wear loss. The reason for the attainment of a stable condition is that ridges and valleys are formed on the surface of the composite during the wear test. These ridges and valleys form due to the interface bonding between the matrix and reinforcement particles. They disappeared as sliding proceeded and were enveloped by wear debris. The COF analysis showed that the percentage

reduction was higher with 12 wt. %B4C addition than in the others, and in all composites, the percentage reduction increased at higher load and longer sliding distance.

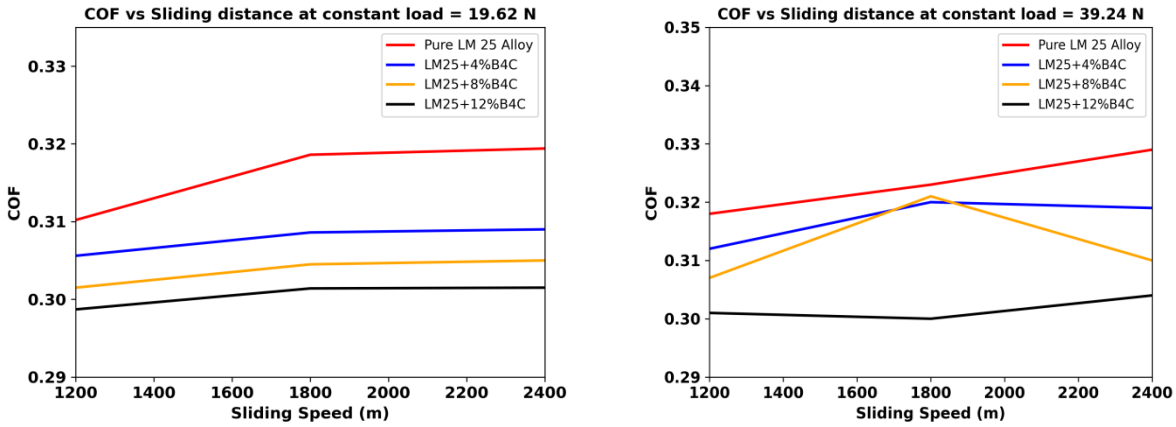


(a) (b)

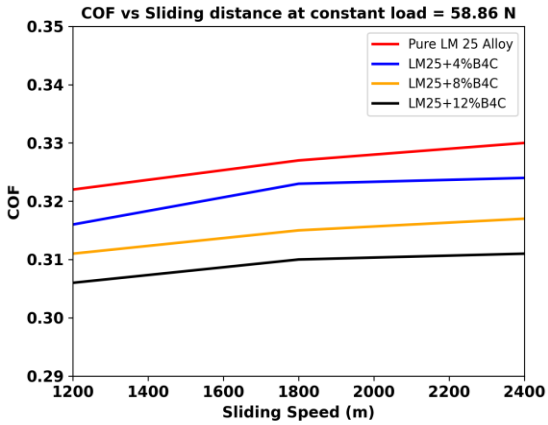


(c)

Figure 8. Plot of the coefficient of friction of the developed composites vs. sliding distance at a constant sliding velocity and different loads (a), 19.62N (b), 38.24N (c), and 58.84N

Figure 9(a) shows the worn surface of the LM25 aluminium alloy composite. The worn surface has grooves parallel to the sliding direction, indicating abrasive wear. The presence of debris indicates that three-body abrasion may have been the cause of abrasive wear. Although two-body abrasion cannot be ruled out because of the hard EN 31-disc, ploughing can be observed at various places. The micrograph shows that the dominating wear mechanism in the cast aluminium alloy is delamination wear, which may have been caused by the presence of plate-like debris and surface fatigue. Figure 9(b) shows the worn surface of the LM25+4 wt.% B4C composite, the micrograph of worn-out surface demonstrates well-defined regions of abrasive wear due to micro-cracking and ploughing along with delamination in the reinforced aluminium alloy composite. Figure 9(c) shows the worn-out surface of aluminium alloy LM25+8 wt.% B4C composite, it is observed that cracks start to initiate around discontinuities, such as hard inclusions and voids created due to a higher percentage of reinforced material. The micrograph also shows a large cavity, which may have developed due to the coalescence of voids. Figure 9(d) shows the worn-out surface of aluminium alloy LM25+12 wt.% B4C composite, it is observed that the surface is deformed plastically which may be caused due to compressive stresses of ceramic particles restrain crack growth in the surface layer. However, some microcracks can also be seen due to ploughing and microcracking in the reinforced aluminium alloy composites. We evaluated the accuracy and variability of the machine learning models used to predict the tribological properties of aluminium-based composites using statistical analyses. In this study, the experimental dataset was divided into 80% for training and 20% for testing. We used the coefficient of determination ($R^2$), mean squared error (MSE), and root mean squared error (RMSE) to assess the model performance on the test data.

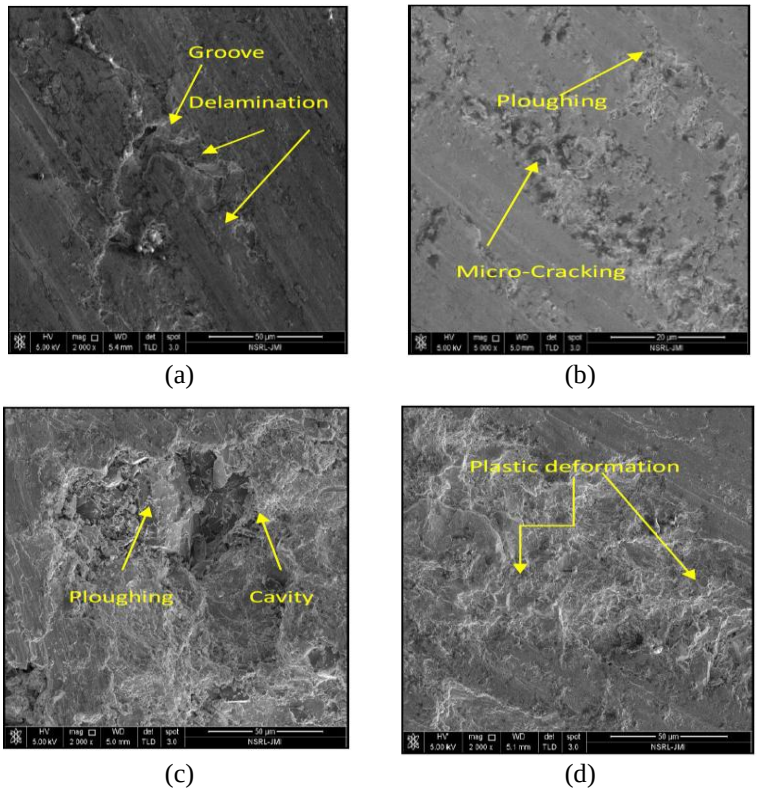


Figure 9. SEM micrograph showing of worn surface analyses for LM 25 alloy and boron B4Ccomposites for 4% 8% and 12%

Figure 10 shows the variation between the predicted and actual values for different machine learning models. The red line represents the reference line (ideal prediction), and the points indicate the predicted values. The dispersion of the predicted data points around the red line serves as an indicator of model accuracy. For the linear regression model, the data points were relatively close to the red line, indicating a moderate level of accuracy. The polynomial regression model showed an even tighter clustering of points near the line, suggesting a higher prediction accuracy compared to linear regression. In contrast, the random forest regression model exhibited data points that lie very close to the red line, which may suggest overfitting, a condition in which the model fits the training data too well but generalises poorly to new data, reducing its practical accuracy. The Gaussian process regression model showed all predicted data points exactly on the red line, which indicates a complete failure of the model, likely due to overfitting or data leakage, resulting in unrealistically perfect predictions that are not generalisable. Among the models, the polynomial regression model demonstrated the highest accuracy in predicting wear properties, followed by the linear regression model, random forest regression, and finally, the Gaussian process regression model, which failed to provide reliable predictions.

Figure 11 illustrates the predicted versus actual values of the coefficient of friction obtained using various machine learning models. Based on the data dispersion in the plots, the linear regression model showed the highest accuracy, followed by the polynomial and random forest regression models. In contrast, the Gaussian process regression model failed to make reliable predictions. Table 8 presents the statistical metrics evaluating the performance of these models for both the wear rate and coefficient of friction. The results indicate varying levels of predictive accuracy depending on the model used. The coefficient of determination ($R^2$) for the wear rate ranged from -0.591 to 0.963, while for the coefficient of friction, it ranged from -0.658 to 0.906. A high $R^2$ value indicates better predictive accuracy, as seen in the polynomial model for wear rate and the linear regression model for the coefficient of friction. Negative $R^2$ values suggest poor model performance, indicating that these models are less accurate than simply using the mean of the observed data.

Table 8. Performance analysis of various models

| | Model | $R^2$ | Mean squared error | Root mean squared error |
|---|---|---|---|---|
| Wear | Linear regression | 0.9 | $2.74\times10^{-6}$ | 0.00160 |
| | Polynomial regression | 0.963 | $1.016\times10^{-6}$ | 0.00100 |
| | Random forest regression | 0.74 | $7.14\times10^{-6}$ | 0.00267 |
| | Gaussian process regression | -0.591 | $4.4\times10^{-5}$ | 0.00660 |
| COF | Linear regression | 0.906 | $5.85\times10^{-6}$ | 0.00240 |
| | Polynomial regression | 0.72 | $1.74\times10^{-5}$ | 0.00420 |
| | Random forest regression | 0.403 | $3.71\times10^{-5}$ | 0.00610 |
| | Gaussian process regression | -0.658 | 0.0001 | 0.01020 |

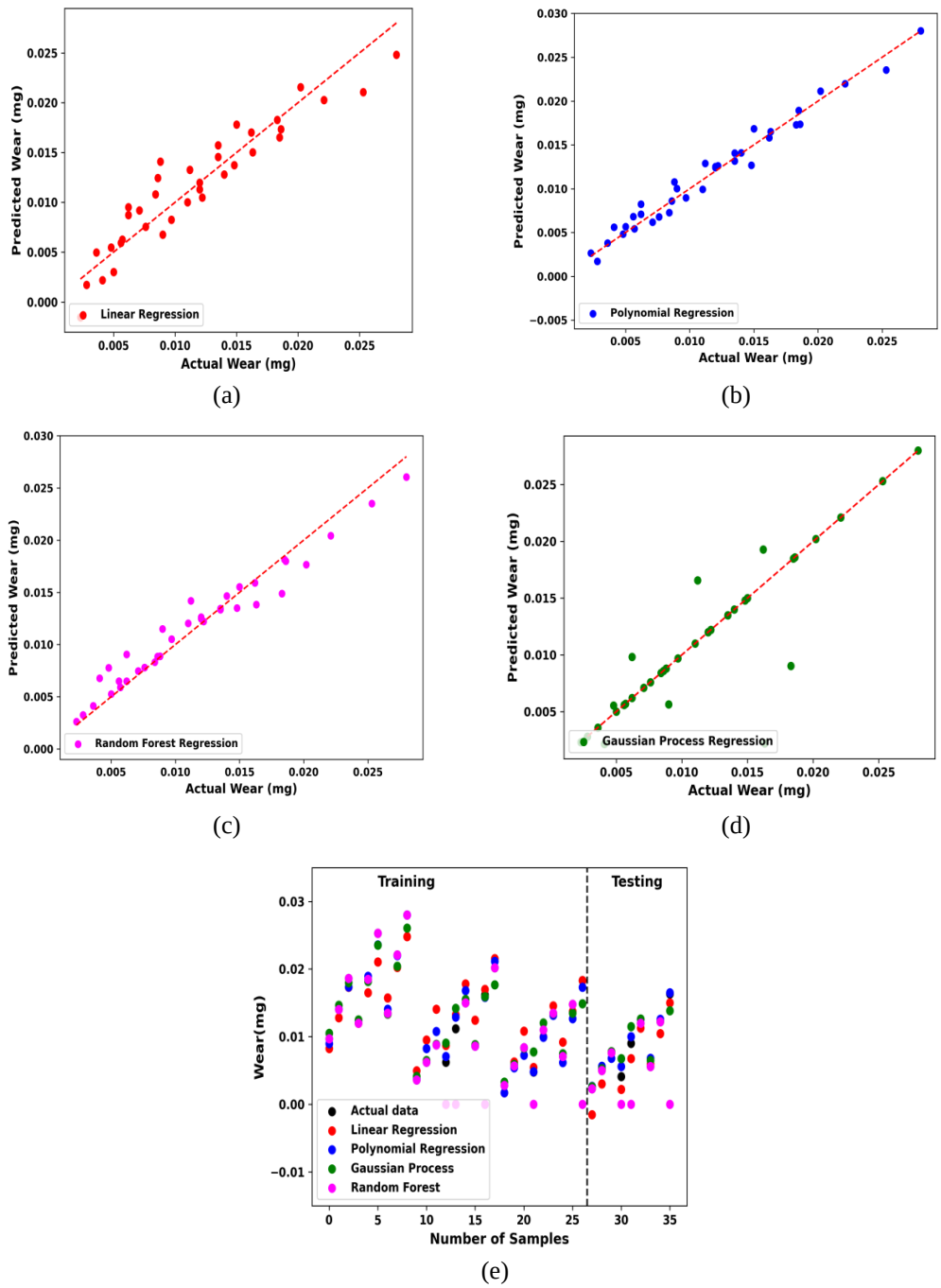


Figure 10. Regression plots for wear rate (a) Linear regression, (b) Polynomial regression, (c) Random forest regression, (d) Gaussian Process Regression, (e) Comparison plot

Generally, when two bodies are in contact and have some relative motion, there is motion, a rise in temperature at the contacting surface of the bodies, and the generated energy is dissipated. The relationship between mass loss in composites and dissipated energy under various loading conditions was studied. The dissipated energy can be calculated using the following relation [44]:

$$E_d = \mu \times W \times v \times t \tag{8}$$

where Ed is the energy dissipated in joules, μ is the average coefficient of friction, W is the normal load in N, v is the sliding velocity in m/s, and t is the total testing duration in s.

Figures 12(a) and (b) show the linear relationship between the mass loss and dissipated energy for the base alloy and all fabricated composites during sliding against EN 31 steel at various loads, and the increase in dissipated energy increased with increasing loads.

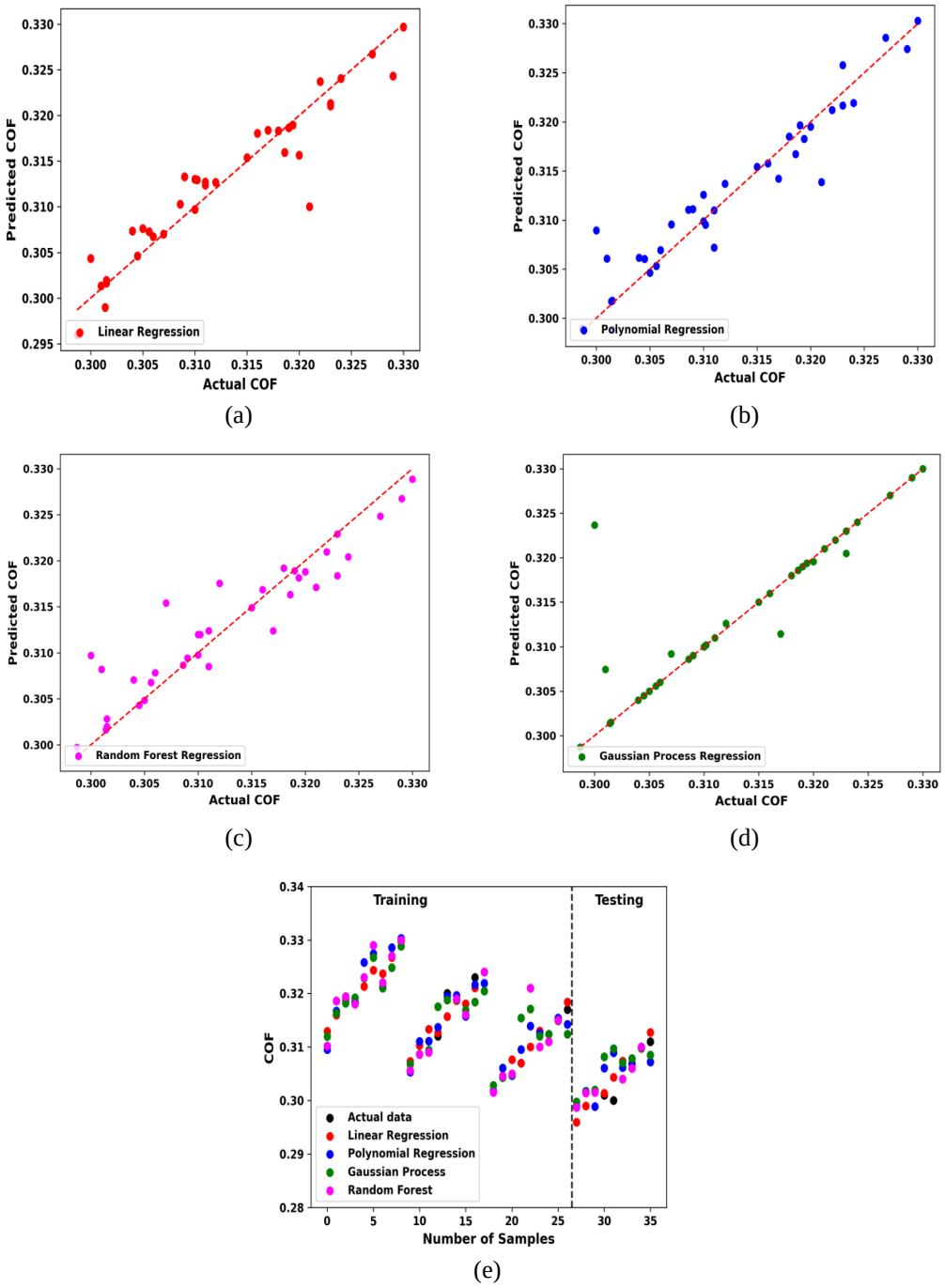


Figure 11. Regression plots for COF (a) Linear regression, (b) Polynomial regression, (c) random forest regression, (d) Gaussian Process Regression, (e) Comparison plot

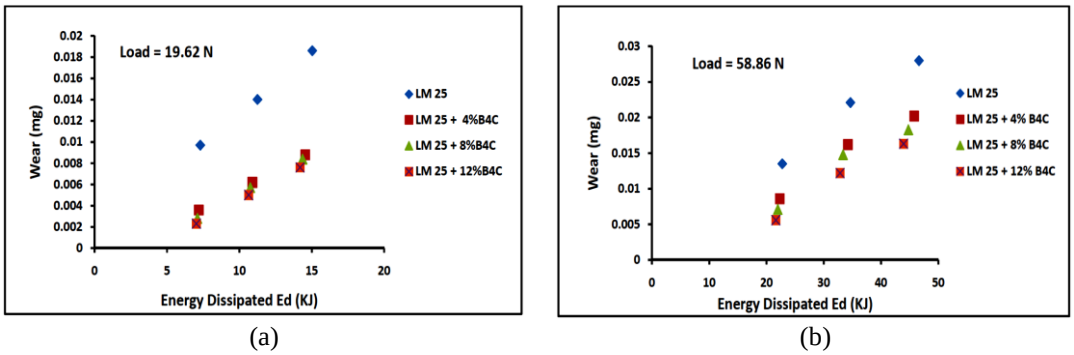


Figure 12. Linear relationship between mass loss and energy dissipated at various loads (a) 19.62 N, (b) 58

## 4. Conclusions

This study investigated the wear behaviour of an aluminium alloy and its composites in combination with an EN 31 steel tribopair under varying loads (19.6–58.86 N) and sliding distances (1200–2400 m), aimed at commercial applications. The Taguchi method was employed to optimise the design of experiments and facilitate the analysis. Additionally, various machine learning models were applied to predict wear and coefficient of friction values based on the input experimental parameters.

i) The design of experiments analysis revealed that the wear rate is most significantly influenced by the percentage of reinforcement, followed by the applied load and sliding distance. The optimal condition for minimising material loss was observed at a reinforcement content of 12 wt.%, a load of 19.62 N, and a sliding distance of 1200 m.

ii) The 12 wt% B4C-reinforced composite exhibited a 21.31% increase in hardness and a 31.05% increase in strength, with brittle tendencies. Micrographs revealed a homogeneous α-aluminium dendrite network structure that developed owing to supercooling during solidification. Brittle morphologies were observed on the fractured surfaces of the 12 wt. %-B4C-added composite, whereas ductile nature was observed for the base and low wt% added composites.

iii) EDS spectrum of LM 25 composites reinforced with 4 wt.% B4C revealed13.62 wt% of boron, 54.48 wt% of carbon, and 31.47 wt% of aluminium, which further increased for boron and decreased for aluminium in the 12 wt.% B4C-added composite. EDS analysis revealed that as the reinforcement percentage increased, the wt.% of hard boron particles increased, improving wear behavior due to their high hardness and compressive strength.

iv) Mass loss reduction was higher at a low load of 19.62 N for 4 wt.% B4C added composite it is reduced to 62.89%, 55.71% and 52.69%, higher for composite reinforced with 8 wt.% and highest for composite sample reinforced with 12 wt.% compared to unreinforced aluminium alloy with increase in sliding distance from 1200m-2400m, similar trend is observed at constant load of 38.24 N and 58.86 N. This is attributed to the dispersion of hard boron carbide particles, which resisted micro-cutting action by acting as load-bearing elements.

v) COF analysis shows that the percentage reduction is higher with 12 wt.% B4C addition than in the other composites, and in all composites, the percentage reduction increased at higher loads and with increasing sliding distance.

vi) Characteristic features of two-body abrasion and ploughing were observed in the base alloy and low-reinforced composites, whereas three-body abrasion and plastic deformation were observed in 12 wt% B4C-reinforced composites; the transition from severe delamination to plastic deformation was attributed to the compressive strength of the hard-ceramic particles, which restrained further wear.

vii) Among the machine learning models evaluated, the polynomial regression model demonstrated the highest accuracy for predicting the wear rate ($R^2$ = 0.963), while the linear regression model performed best for predicting the coefficient of friction.

viii) A relationship was observed between the mass loss and dissipated energy under varying loads, and a linear increasing trend was observed for all the composite samples against the dissipated energy at various loads. The change in the amount of dissipated energy was almost negligible for all the composite samples compared with steel EN 31 and increased with increasing loads.

**Acknowledgements**

The authors acknowledge the support of the Department of Mechanical Engineering, R V Institute of Technology, Bijnor, Uttar Pradesh, India, for providing facilities for this research.

**Funding**

This study was not supported by any grants from funding bodies in the public, private, or not-for-profit sectors.

**Declaration of Competing Interests**

The authors declare no conflicts of interest.

**CRediT Author Contribution Statement**

Zeeshan Ahmad: Conceptualisation; Methodology; Investigation; Writing – original draft
Sabah Khan: Conceptualization; Analysis; Investigation; Validation; Supervision; Writing – review & revise

**Availability of Data and Materials**

The datasets generated and/or analysed in the current study are available from the corresponding author upon reasonable request.

**Ethics Statement**

This study did not involve human participants or animal subjects. Therefore, this study did not require ethical approval.

**Generative Artificial Intelligence Disclosure**

Artificial intelligence tools [ChatGPT Plus] were used to assist with literature summarisation, language refinement, and readability. All AI-generated content was reviewed and verified by the authors for accuracy and originality. The authors are solely responsible for the final interpretation and conclusions.

**References**


[1] M. K. Surappa, "Aluminium matrix composites: Challenges and opportunities," *Sadhana*, vol. 28, nos. 1–2, pp. 319–334, 2003, https://doi.org/10.1007/BF0271714.

[2] H. Tan, S. Wang, J. Cheng, S. Zhu, and J. Yang, "Sliding tribological behavior of Al–Fe–V–Si–graphite solid-lubricating composites at elevated temperatures," *Journal of Tribology*, vol. 140, no. 1, Art. no. 011302, 2018, https://doi.org/10.1115/1.4037213.

[3] S. V. Prasad and R. Asthana, "Aluminum metal-matrix composites for automotive applications: Tribological considerations," *Tribology Letters*, vol. 17, no. 3, pp. 445–453, 2004, https://doi.org/10.1023/B:TRIL.0000044492.91991.f3.

[4] S. Ramarao and G. Padmanabhan, "Fabrication and mechanical properties of aluminium-boron carbide composites," *International Journal of Materials and Biomaterials Applications*, vol. 2, no. 3, p. 15, 2012.

[5] U. B. G. Krishna, K. V. S. Rao, and B. Vasudeva, "Effect of percentage reinforcement of $B_4C$ on the tensile property of aluminium matrix composites," *International Journal of Mechanical Engineering and Robotics Research*, vol. 1, no. 3, pp. 290–295, 2012.

[6] A. Baradeswaran and A. Elaya Perumal, "Influence of $B_4C$ on the tribological and mechanical properties of Al 7075–$B_4C$ composites," *Composites Part B: Engineering*, vol. 54, pp. 146–152, 2013, https://doi.org/10.1016/j.compositesb.2013.05.012.

[7] N. Subramani, K. Vijayaraghavan, V. V. Arunsankar, and K. Sudha, "Analysis and investigation on A2024 metal matrix composites with $B_4C$ and graphite," *International Journal of Innovative Research in Science, Engineering and Technology*, vol. 2, no. 9, pp. 4636–4642, 2013.

[8] Z. Ahmad, S. Khan, and S. Hasan, "Microstructural characterization and evaluation of mechanical properties of silicon nitride reinforced LM 25 composite," *Journal of Materials Research and Technology*, vol. 9, no. 4, pp. 9129–9135, 2020, https://doi.org/10.1016/j.jmrt.2020.06.037.

[9] B. Rebba and N. Ramanaiah, "Studies on mechanical properties of 2024 Al–$B_4C$ composites," *International Journal of Advanced Materials Manufacturing and Characterization*, vol. 4, no. 1, pp. 42–46, 2014, https://doi.org/10.11127/ijammc.2014.03.06.

[10] T. Raviteja, N. Radhika, and R. Raghu, "Fabrication and mechanical properties of stir cast Al-Si12Cu/$B_4C$ composites," *International Journal of Research in Engineering and Technology*, vol. 3, no. 7, pp. 343–346, 2014, https://doi.org/10.15623/ijret.2014.0307058.

[11] N. Yuvaraj, S. Aravindan, and Vipin, "Fabrication of Al5083/$B_4C$ surface composite by friction stir processing and its tribological characterization," *Journal of Materials Research and Technology*, vol. 4, no. 4, pp. 398–410, 2015, https://doi.org/10.1016/j.jmrt.2015.02.006.

[12] R. Harichandran and N. Selvakumar, "Effect of nano/micro $B_4C$ particles on the mechanical properties of aluminium metal matrix composites fabricated by ultrasonic cavitation-assisted solidification process," *Archives of Civil and Mechanical Engineering*, vol. 16, no. 1, pp. 147–158, 2016, https://doi.org/10.1016/j.acme.2015.07.001.

[13] J. A. Qayyum, K. Altaf, A. Mahmood, M. Shah, and A. M. A. Rani, "Grain refinement of LM25 aluminum alloy casting using sloping plate process," *ARPN Journal of Engineering and Applied Sciences*, vol. 11, no. 22, pp. 13049–13052, 2016.

[14] S. Khan and Z. Ahmad, "Comparative analysis for coefficient of friction of LM 25 alloy and LM 25 granite composite at different sliding speeds and applied pressure," *International Journal of Mechanical and Production Engineering Research and Development*, vol. 8, no. 3, pp. 291–300, 2018, https://doi.org/10.24247/ijmperdjun201833.

[15] M. Vilaseca, S. Molas, and D. Casellas, "High temperature tribological behaviour of tool steels during sliding against aluminium," *Wear*, vol. 272, no. 1, pp. 105–109, 2011, https://doi.org/10.1016/j.wear.2011.07.007.

[16] J. Pujante, L. Pelcastre, M. Vilaseca, D. Casellas, and B. Prakash, "Investigations into wear and galling mechanism of aluminium alloy–tool steel tribopair at different temperatures," *Wear*, vol. 308, no. 1–2, pp. 193–198, 2013, https://doi.org/10.1016/j.wear.2013.06.015.

[17] A. Zavos and P. Nikolakopoulos, "Effects of surface irregularities on piston ring–cylinder tribo pair of a two-stroke motor engine in hydrodynamic lubrication," *Tribology in Industry*, vol. 37, no. 1, pp. 1–12, 2015.

[18] K. M. Chen, Y. Zhou, X. X. Li, Q. Y. Zhang, L. Wang, and S. Q. Wang, "Investigation on wear characteristics of a titanium alloy/steel tribo-pair," *Materials & Design*, vol. 65, pp. 65–73, 2015, https://doi.org/10.1016/j.matdes.2014.09.016.

[19] H. Li, G. Zhang, and L. Wang, "The role of tribo-pairs in modifying the tribological behavior of the $MoS_2$/Ti composite coating," *Journal of Physics D: Applied Physics*, vol. 49, no. 9, Art. no. 095501, 2016, https://doi.org/10.1088/0022-3727/49/9/095501.

[20] P. C. Reddy, S. Arumugam, P. N. S. Krishna, and N. J. Sainath, "Tribological investigation of a compressor liner-ring material under various bio-based lubricants using HFRR tribometer," *IOP Conference Series: Materials Science and Engineering*, vol. 390, no. 1, Art. no. 012025, 2018, https://doi.org/10.1088/1757-899X/390/1/012025.

[21] E. Huttunen-Saarivirta, L. Kilpi, T. J. Hakala, J. Metsäjoki, and H. Ronkainen, "Insights into the behaviour of tool steel–aluminium alloy tribopair at different temperatures," *Tribology International*, vol. 119, pp. 567–584, 2018, https://doi.org/10.1016/j.triboint.2017.11.041.

[22] B. Stojanović, M. Babić, S. Veličković, and J. Blagojević, "Tribological behavior of aluminum hybrid composites studied by application of factorial techniques," *Tribology Transactions*, vol. 59, no. 3, pp. 522–529, 2016, https://doi.org/10.1080/10402004.2015.1091535.
[23] L. Wang, J. Cai, J. Zhou, and J. Duszczyk, "Characteristics of the friction between aluminium and steel at elevated temperatures during ball-on-disc tests," *Tribology Letters*, vol. 36, no. 2, pp. 183–190, 2009, https://doi.org/10.1007/s11249-009-9475-x.
[24] Z. Ahmad, S. Khan, R. C. Cozza, R. Penchaliah, and V. Verma, "Assessment of the tribological behavior of a metallic tribopair: LM25 alloy–$Si_3N_4$ composites against EN 31 steel," *Materials Today: Proceedings*, vol. 67, no. 2, pp. 431–437, 2022, https://doi.org/10.1016/j.matpr.2022.08.031.
[25] Y. Sahin, "Optimization of testing parameters on the wear behaviour of metal matrix composites based on the Taguchi method," *Materials Science and Engineering: A*, vol. 408, no. 1–2, pp. 1–8, 2005, https://doi.org/10.1016/j.msea.2004.11.012.
[26] A. Afzal, S. A. Khan, M. T. Islam, R. D. Jilte, A. Khan, and M. E. M. Soudagar, "Investigation and back-propagation modeling of base pressure at sonic and supersonic Mach numbers," *Physics of Fluids*, vol. 32, no. 9, Art. no. 096109, 2020, https://doi.org/10.1063/5.0022015.
[27] M. N. Akhtar, T. Sathish, V. Mohanavel et al., "Optimization of process parameters in CNC turning of aluminum 7075 alloy using L27 array-based Taguchi method," *Materials*, vol. 14, no. 16, Art. no. 4470, 2021, https://doi.org/10.3390/ma14164470.
[28] A. Afzal, A. D. M. Samee, R. D. Jilte, M. T. Islam, A. M. Manokar, and K. A. Razak, "Battery thermal management: An optimization study of parallelized conjugate numerical analysis using cuckoo search and artificial bee colony algorithm," *International Journal of Heat and Mass Transfer*, vol. 166, Art. no. 120798, 2021, https://doi.org/10.1016/j.ijheatmasstransfer.2020.120798.
[29] M. Meignanamoorthy, M. Ravichandran, V. Mohanavel et al., "Microstructure, mechanical properties, and corrosion behavior of boron carbide reinforced aluminum alloy (Al-Fe-Si-Zn-Cu) matrix composites produced via powder metallurgy route," *Materials*, vol. 14, no. 15, Art. no. 4315, 2021, https://doi.org/10.3390/ma14154315.
[30] T. H. M. Mysore, A. Y. Patil, G. U. Raju et al., "Investigation of mechanical and physical properties of big sheep horn as an alternative biomaterial for structural applications," *Materials*, vol. 14, no. 14, Art. no. 4039, 2021, https://doi.org/10.3390/ma14144039.
[31] T. Sathish, A. R. R. Kaladgi, V. Mohanavel et al., "Experimental investigation of the friction stir weldability of AA8006 with zirconia particle reinforcement and optimized process parameters," *Materials*, vol. 14, no. 11, Art. no. 2782, 2021, https://doi.org/10.3390/ma14112782.
[32] I. G. Crouch, G. V. Franks, C. Tallon, S. Thomas, and M. Naebe, "Glasses and ceramics," in *The Science of Armour Materials*, I. G. Crouch, Ed. Cambridge, U.K.: Woodhead Publishing, 2017, pp. 331–393, https://doi.org/10.1016/B978-0-08-100704-4.00007-4.
[33] T. V. Vardhan, U. Nagaraju, G. H. Gowd, and V. Ajay, "Evaluation of properties of LM 25–alumina–boron carbide MMC with different ratios of compositions," *International Journal of Applied Engineering Research*, vol. 12, no. 14, pp. 4460–4467, 2017.
[34] Z. Ahmad and S. Khan, "Mechanical characterization of LM25 alloy matrix composite reinforced with boron carbide," *Journal of Composite Materials*, vol. 55, no. 22, pp. 3151–3158, 2021, https://doi.org/10.1177/00219983211005513.
[35] Z. Ahmad, H. Z. Jafri, and R. H. Basha, "Characterization techniques for composites using AI and machine learning techniques," in *Computational Technologies in Materials Science, S. Tayal, P. Singla, A. Nandi, and J. P. Davim, Eds.* Boca Raton, FL, USA: CRC Press, 2021, pp. 139–167. https://doi.org/10.1201/9781003121954-7.
[36] S. C. Tjong and K. C. Lau, "Abrasive wear behavior of $TiB_2$ particle-reinforced copper matrix composites," *Materials Science and Engineering: A*, vol. 282, no. 1–2, pp. 183–186, 2000, https://doi.org/10.1016/S0921-5093(99)00752-2.
[37] A. Canakci and F. Arslan, "Abrasive wear behaviour of $B_4C$ particle reinforced Al2024 MMCs," *The International Journal of Advanced Manufacturing Technology*, vol. 63, no. 5–8, pp. 785–795, 2012, https://doi.org/10.1007/s00170-012-3931-8.
[38] M. Kök, "Abrasive wear of $Al_2O_3$ particle reinforced 2024 aluminium alloy composites fabricated by vortex method," *Composites Part A: Applied Science and Manufacturing*, vol. 37, no. 3, pp. 457–464, 2006, https://doi.org/10.1016/j.compositesa.2005.05.038.
[39] A. T. Alpas, H. Hu, and J. Zhang, "Plastic deformation and damage accumulation below the worn surfaces," *Wear*, vol. 162–164, pp. 188–195, 1993, https://doi.org/10.1016/0043-1648(93)90500-L.
[40] K. R. Suresh, H. B. Niranjan, P. M. Jebaraj, and M. P. Chowdiah, "Tensile and wear properties of aluminum composites," *Wear*, vol. 255, no. 1–6, pp. 638–642, 2003, https://doi.org/10.1016/S0043-1648(03)00292-8.
[41] S. Das, S. Das, and K. Das, "Abrasive wear of zircon sand and alumina reinforced Al–4.5 wt% Cu alloy matrix composites—A comparative study," *Composites Science and Technology*, vol. 67, no. 3–4, pp. 746–751, 2007, https://doi.org/10.1016/j.compscitech.2006.05.001.
[42] D. Kumar, H. Roy, and B. K. Show, "Tribological behavior of an aluminum matrix composite with $Al_4SiC_4$ reinforcement under dry sliding condition," *Tribology Transactions*, vol. 58, no. 3, pp. 518–526, 2015, https://doi.org/10.1080/10402004.2014.990594.

[43] P. Kumar and M. F. Wani, "Tribological characterization of hypereutectic Al–25Si alloy under dry and lubricated sliding conditions," *Journal of Tribology*, vol. 140, no. 1, Art. no. 011603, 2018, https://doi.org/10.1115/1.4036918.
[44] E. Marui, M. Hashimoto, S. Kato, and W. Kojima, "Dissipation of kinematic energy by slip at the interface of mating surfaces," *Wear*, vol. 159, no. 1, pp. 141–150, 1992, https://doi.org/10.1016/0043-1648(92)90296-K.
[45] M. Z. Huq and J. P. Celis, "Reproducibility of friction and wear results in ball-on-disc unidirectional sliding tests of TiN–alumina pairings," *Wear*, vol. 212, no. 2, pp. 151–159, 1997, https://doi.org/10.1016/S0043-1648(97)00167-1.
[46] H. Czichos, D. Klaffke, E. Santner, and M. Woydt, "Advances in tribology: The materials point of view," *Wear*, vol. 190, no. 2, pp. 155–161, 1995, https://doi.org/10.1016/0043-1648(96)80014-7.